Sustained Flexible Photonic Transistor Memories

Based on Fully Natural Floating Gate Electret

Chun-Kai Chen,[a,b] *Jin-Chieh Ho,*[a,b] *Chih-Chien Hung,* [a,b] *Wei-Cheng Chen,*[a,b]

Toshifumi Satoh,[c*] *and Wen-Chang Chen* [a,b*]

[a] Department of Chemical Engineering, National Taiwan University, No. 1, Sec. 4, Roosevelt Rd., Taipei 10617, Taiwan.

[b] Advanced Research Center for Green Materials Science and Technology, National Taiwan University, No. 1, Sec. 4, Roosevelt Rd., Taipei 10617, Taiwan.

[c] Faculty of Engineering, Hokkaido University, N13W8, Kita-ku, Sapporo 060-8628, Japan.

[*] To whom all correspondence should be addressed: T. Satoh (E-mail: satoh@eng.hokudai.ac.jp) and W.-C. Chen (E-mail: chenwc@ntu.edu.tw)

Key words: hemin; porphyrin; degradable; polylactic; photonic memory

Abstract

Photonic transistor memory with high-speed communication and energy-saving capabilities has emerged as a new data storage technology. However, most floating-gate electrets are composed of quantum dots derived from petroleum or metals, which are either toxic or harmful to the environment. In this study, an environmentally friendly floating-gate electret made entirely from biomass-derived materials was designed for photonic memory. The results show that the photosensitive hemin and its derivative protoporphyrin IX (PPIX) were successfully embedded in a polylactic acid (PLA) matrix. Correspondingly, their disparate photochemistry and core structure strongly affected the photosensitivity and charge-trapping capacity of the prepared electrets. With an appropriate energy-level alignment, the interlayer exciton formed with the correct alignment of energy levels within the PPIX/PLA electret. In addition, the demetallized core offered a unique relaxation dynamic and additional trapping sites to consolidate the charges. Correspondingly, the as-prepared device exhibited a memory ratio of up to 2.5×10^7 with photo-writing-electrical-erasing characteristics. Conversely, hemin demonstrated self-charge transfer during relaxation, making it challenging for the device to store the charges and exhibit a photorecovery behavior. Furthermore, the effect of trapping site discreteness on memory performance was also investigated. The photoactive components were effectively distributed due

to the high dipole-dipole interaction between the PLA matrix and PPIX, resulting in a sustained memory performance for at least 10^4 s after light removal. The photonic memory was also realized on a bio-derived dielectric flexible substrate. Accordingly, a reliable photorecording behavior was observed, wherein, even after 1000 cycles of bending under a 5-mm bending radius, the data was retained for more than 10^4 s. To our knowledge, it is the first time that a two-pronged approach has been used to improve the performance of photonic memory while addressing the issue of sustainability with a biodegradable electret made entirely from natural materials.

Introduction

Following significant advancements in the Internet of Things and mobile electronics, high-speed communication-capable data storage technologies are urgently desired in the modern era.[1] Consequently, the focus of research on electrically-driven devices has shifted from Von Neumann architecture and energy conservation to light programming.[2] In addition, the rapid development of emerging technologies has generated a great deal of enthusiasm for the pursuit of portable electronics that can be realized on flexible substrates.[3,4] Correspondingly, flexible photoresponsive organic field-effect transistor (OFET) memory has sparked significant research interest in next-generation electronics. OFET memory inspection has several advantages,

including high discriminability, nondestructive readout, and excellent compatibility with complementary metal-oxide semiconductors.[5] Currently, floating-gate dielectrics,[6,7] D-A polymer electrets,[8] semiconducting composites,[9] and upconverting nanoparticle hybrid systems[10,11] are employed in light-triggered OFET memory. Accordingly, photoactive components are mixed with an insulating gate dielectric to create a floating-gate system, resulting in a promising and facile approach for designing chargeable electrets. Until now, the development of floating-gate dielectric has relied on nonrenewable or metallic materials,[10,11] that are either toxic or environmentally unfriendly. Additionally, the increasing use of petroleum-based sources in electronics production causes severe environmental pollution. Furthermore, with the explosive growth of electronic waste, the short lifespan of memory devices inherently results in an ecological problem.[12] To address these issues and promote sustainability, it is, therefore, necessary to incorporate renewable or degradable materials. Moreover, implementing a biomaterial-based memory device with durable data storage behavior would be indispensable for next-generation electronics.

As a promising photoactive heterocyclic group, porphyrin exhibits several naturally occurring derivatives, such as chlorophyll, vitamin B_{12}, and hemin.[13] Their structural peculiarities, including extensive π-conjugated tetrapyrrole scaffold and various peripheral substituents on the

pyrrole ring, confers intense absorption, stable photochemical properties, and structural designability.[14,15] Correspondingly, research on porphyrin-based materials has accelerated the growth of optoelectronic technologies such as photonics sensors,[16] organic photovoltaic cells,[17] and synaptic transistors.[18,19] In this regard, Huang et al. reported chlorophyll-based neuromorphic computing devices with long-term air stability and degradability,[19] which benefit from the solid absorption of the Soret band, resulting in an enhancement in the overall photoresponsivity of the device.[20] Correspondingly, porphyrin-based chemicals derived from natural organisms have emerged as promising candidates for developing bio-safe optoelectronics. Hemin, an iron(III)-containing porphyrin-based chemical, was first synthesized from defibrinated beef blood in 1941.[21] Due to its intriguing photochemistry, thermal resistance, and cost-effectiveness, it is widely employed in pharmacology,[22] enzyme catalysis,[23] and in the fabrication of biological sensors.[24] Since the electron-rich π-system and the coordinated iron complex endow hemin with significant redox properties,[25] we envisaged that the significant intramolecular charge distribution between hemin molecules could affect their charge-trapping capacity. Protoporphyrin IX (PPIX), devoid of a coordinated iron(III) ion, can be produced by irradiating the metal-ligand cleavage of hemin derived from biomass.[26] In this regard, Gellini et al. determined the relaxation dynamics of hemin and PPIX from the excited state to the ground state and interpreted the transient evolution

following the excitation of the Soret band.[27] In addition, the existence of a central metal ion was found to impart a substantial effect on the photochemical properties of PPIX,[28] which is a crucial aspect of photoresponsivity and charge storage behavior in photonic memory.

This study reports the development of a floating-gate electret made entirely from biomass for photonic OFET memories. The bio-electret includes photoactive components such as hemin and its derivative PPIX and a polylactic acid (PLA) matrix with mechanical ductility and degradability[29]. Especially, we emphasize two bio-electret-based memory systems, hemin/PLA and PPIX/PLA to realize the electrical properties under electrical stress and light irradiation. In addition, the discreteness of trapping sites in photoactive components is intensively studied via modulating the blending ratio, processing solvent, and types of the polymer matrix. We also investigated the photochemistry of each photoactive component and pentacene/bio-electret bilayers to gain a deeper understanding of the working principles of the study electrets. The corresponding operating mechanisms in bio-electret photoresponsivity, charge formation, and charge storage persistence are proposed. Furthermore, the discreteness of trapping sites in photoactive components was studied in depth by modulating the blending ratio, processing solvent, and polymer matrix types. Finally, we demonstrated that the substrate and gate dielectrics of the bio-electret that was integrated into fully flexible electronics were derived from

using biomass-based polymers. To our knowledge, this is the first time that the effect of metal ion insertion in bio-derived porphyrin-based chemicals on photonic memory performance has been investigated. This work unequivocally demonstrates the bright and sustainable future of bio-derived and biodegradable electret in next-generation data storage technology.

Experimental Section

Materials. All reagents and solvents were used as received from commercial sources. Hemin (90%), extracted from bovines, PPIX 95%, PLA M_w~60,000 $gmol^{-1}$), polystyrene (PS, M_w~35,000 g mol^{-1}), anhydrous 1-methyl-2-pyrrolidone (NMP, 99.5%), and anhydrous chloroform (CF, 99%) were purchased from Merck (90%, U.S.A.) to prepare the chargeable electrets. Pentacene (99%, Merck, U.S.A.) was used as an active layer for field-effect transistor (FET) devices. For the demonstration of flexible FET memory, the reported biomass-based polyimide (PI)[30] was derived from (3*R*,6*S*)-hexahydrofuro[3,2-*b*]furan-3,6-diyl bis(4-aminobenzoate) (ISBA) and 4,4'-biphthalic anhydride [BPDA, >98%, TCI (Japan)], and served as the flexible substrate and gate dielectric.

Device fabrication. The photonic transistor-type memories using a highly n-doped silicon wafer or flexible PI as the substrate were based on a bottom gate top contact configuration.

Hemin (20 mg) or PS was dissolved in 1 ml of anhydrous NMP or CF. Subsequently, different ratios of PLA or PS polymer solution (20 mg/ml in anhydrous NMP or CF as solvent) were added to this solution. The as-obtained solutions were then filtered through a PTFE membrane syringe filter and spin-coated onto a highly n-doped silicon wafer with a 100-nm thick SiO_2 gate dielectric at 2000 rpm for 60 s. The polymer-thin film was then annealed at 60 °C for 30 min under vacuum. For the transporting layer, 50-nm-thick pentacene was deposited at a rate of 0.3 $Å s^{-1}$ at 10^{-7} torr. Finally, a 65-nm-thick Au was deposited under the same conditions through the regular shadow mask for the source and drain electrodes, with a channel length of 50 m and a channel width of 1000 μm. Concerning the flexible OFET memory, the biomass-based PI was used as a flexible substrate and gate dielectric. Accordingly, the PI film was first deposited using a 65-nm-thick Au through the regular shadow mask for the gate electrode. The PI precursor (20 wt.% in anhydrous NMP as solvent) was then spin-coated onto the substrate and imidized successively under vacuum at 100, 200, and 300 for 1 h. Thus, the study electret, pentacene transporting layer, and Au top electrodes, referred to in the aforementioned conditions, were fabricated.

Results and discussions

The effect of iron(III) ion presence on memory performance. The schematic structure of the photonic FET memory, in which the photoactive electret is composed of bio-based PLA as the polymeric matrix and hemin or PPIX as the photoactive components, is illustrated in **Figure 1a**. As observed, the studied electrets were integrated between a SiO_2 dielectric and a p-type transporting layer composed of pentacene. Hemin is a natural iron(III) ion-containing porphyrin complex that can be extracted from bovine cells. Correspondingly, freebase PPIX, which lacks coordinated iron(III) ions, can be converted from hemin by ultrasound irradiation. The detailed fabrication procedure for the device is described in the experimental section. Numerous researchers have studied the photochemistry of porphyrin-based chemicals and integrated them into various optoelectronics. To investigate the photoresponse or photostorage properties of the studied photoactive components, two types of photoactive electrets prepared with hemin and PPIX were thoroughly analyzed. The purpose of the devices comprised bio-based photoactive components/PLA with a blending ratio of 1/2 as electret is to observe memory switching behaviors (**Figures 1b** and **1d**) and memory retention (**Figures 1c** and **1e**). The p-channel FET transfer and output curves are presented in **Figure S1,** and the relevant device parameters and memory performances are summarized in **Table S1**. For light source operation, all characterizations were captured in a pitch-black environment. In addition, the

FET characteristics were estimated by sweeping the gate voltage (V_G) from 10 to −60 V with the drain voltage (V_D) held constant at −60 V. As shown in **Figure S1**, significant hysteresis occurred, indicating a polarization mechanism in the initial state (dark). Subsequently, the transfer characteristics were recorded under electrically programmed stress or light illumination to investigate the performance of photonic memory further. Accordingly, an appropriate V_G pulse was applied for electrical writing purposes, and the transfer curves for both electrets shifted in a negative direction when subjected to a V_G pulse of −60 V for 1 s. The charge storage capability of the electret is represented by the deviated onset of transfer curves caused by the modification of the conducting channel. Therefore, an appropriate V_G pulse was applied for electrical writing purposes. As observed, the transfer curves for both electrets shifted in a negative direction when subjected to a V_G pulse of −60 V for 1 s. Moreover, the PPIX/PLA-based device exhibited a negative threshold voltage (V_{TH}) shift of 5 V, which could be explained by the band diagram in **Figure 2a**. Subsequently, the relevant wavelength of maximum energy absorption (λ_{max}) and solid-state band gap (E_g) of the studied materials were determined from their ultraviolet−visible absorbance spectra (**Figure 2b**). As observed, hemin and PPIX exhibited similar λ_{max} (401 and 406 nm) and E_g values (2.57 and 2.51 eV). In addition to the above, the highest occupied molecular orbital (HOMO) and lowest

occupied molecular orbital (LUMO) energy levels of the studied materials relative to ferrocene were estimated from the onset of their oxidation (**Figure S2**). As evident from the figure, the HOMO and LUMO levels of hemin and PPIX were −5.29 and −5.14, as well as −2.72 and −2.63 eV, respectively. Without iron(III) coordination, PPIX possessed a free –N–H– group that donates electrons and endows destabilized frontier orbitals contributing to higher HOMO and LUMO levels. However, due to the greater difference between the HOMO levels of pentacene (5.22 eV), PPIX (5.14 eV), and hemin (5.29 eV), the induced hole carriers from the transporting layer can overcome the barrier very easily. Correspondingly, the electrical stress injects hole carriers into the chargeable electret, resulting in a more robust switching behavior.

To determine the photoresponse or photostorage characteristics, the device was subsequently characterized under blue light (405 nm, 0.95 $mWcm^{-2}$) irradiation for multiple exposure intervals. After exposure to light for 5 and 60 s, respectively, the transfer curve of the hemin/PLA-based device was found to shift back to the original trace or a more positive voltage region. In addition, the photoactive hemin generated Frenkel excitons under the influence of light, and the dissociated holes were released by coulombic force at the electrets/pentacene interface, returning to the transporting layer.[31] Moreover, the left counterpart of electrons was maintained, which modified the polarity of a conductive channel

to produce photorecovery and photoprogrammable behaviors in hemin/PLA and PPIX/PLA-based devices, respectively. However, the PPIX/PLA-based device demonstrated a more unusual switching behavior for shorter light irradiation of 5 s. During this time, the transient current increased considerably, and a memory ratio (I_{ON}/I_{OFF}) of 5.2×10^3 was recorded at V_G = 0 V, thus, presenting an excellent value. In contrast, the hemin/PLA-based device exhibited a significantly lower I_{ON}/I_{OFF} of 3.7×10^1, even when photo-driven for 60 s. Thus, with a shorter light exposure time and a respectable memory ratio, PPIX, the photoactive component in the electret, was found to be more suitable for photo programming. For the transient characteristics, the temporal source→drain current (I_{DS}) was recorded with a fixed V_D of −60 V and V_G of 0 V under dark conditions. Subsequently, the light illumination process was analyzed at various time intervals (blue-filled area; 1−60s). Accordingly, we determined the initial and photoprogramming states to be the “OFF” and “ ON” states based on their recorded current. This suggests that the device has a high performance with a higher ($I_{ON/OFF}$) ratio under shorter light exposure times. As shown in Figures 1c and 1e, the I_{DS} of the hemin/PLA electret-based device decreased gradually after light removal. Furthermore, even when illuminated for an extended 60 s, the hemin/PLA electret had difficulty retaining the trapped charges. In contrast, the PPIX/PLA-based device exhibited a stable photorecording behavior with a well-preserved

I_{DS} after removing the light source. The band diagram and photochemistry of the studied photoactive components can elucidate the difference in the photostorage performance of hemin/PLA and PPIX/PLA electret. First, it is simple to identify the greater difference between the LUMO levels of pentacene (−3.45 eV), PPIX (−2.63 eV), and hemin (−2.72 eV), which prevents trapped electrons from returning to the transporting layer. Secondly, due to the adequate alignment in energy level between pentacene and PPIX/PLA electret, the bandgap of 1.69 eV between the LUMO level of pentacene and the HOMO level of PPIX facilitates interlayer charge recombination, which generates the excitons for external stimulus to the electret.[32] Thus, more Frenkel excitons were generated, and more electrons with their left-handed counterparts were retained in the electret, giving the device a larger conductive channel and a higher memory ratio. To corroborate the formation of an interlayer exciton, the PL spectra of the pure studied photoactive components (solid line) and double-layer with deposited pentacene on the studied photoactive components (dashed-line) were investigated (**Figure 2c**). As observed, the thin films of the photoactive components were excited by 405 nm light, and both exhibited emission peaks at 560 nm; PPIX also exhibited an additional emission peak at 700 nm. However, there was no light absorbance at 700 nm in the PPIX/PLA electret (**Figure 2b**) or pentacene, thereby ruling out the possibility that the light emission

from PPIX was absorbed by the transporting layer or by itself. Inferring from the PL spectra of photoactive component-pentacene double-layer films on quartz, hemin/PLA-pentacene exhibited similar PL emission characteristics as pure hemin films. Conversely, PPIX/PLA-pentacene exhibited an additional emission peak at 705 nm and a 68% increase in PL intensity. In contrast, the 1.84 eV bandgap between the LUMO level of pentacene and the HOMO level of hemin prevented their charges from recombining. As a result, the memory ratio of the hemin/PLA-based device was quite low. In an earlier study, Gellini et al. investigated the relaxation pathway of hemin and PPIX from an excited to a ground state.[27] Accordingly, hemin was reported to possess faster relaxation rates due to charge transfer; on the other hand, PPIX was reported to relax through internal conversion and vibrational relaxation, which could be ascribed to the insertion of iron(III) ion to activate the relaxation channels from the $\pi \rightarrow \pi^*$ state in the porphyrin ring to the center of the metal ion. Thus, the trapped charges in the hemin/PLA electret tend to dissipate via self-charge transfer, resulting in diminished memory persistence. If the hemin/PLA-based device was continuously driven by light illumination (**Figure 1b**), a compatible I_{ON}/I_{OFF} ratio of 1.1×10^3 is observed. Since photo-driven excitons are continuously generated, they compensate for the electron lost during charge transfer between hemin molecules. Consequently, the conductance of the active channel is maintained.

This result, therefore, demonstrates the strong correlation between the memory properties of hemin and its photochemistry. To gain more insight into the device-to-device variations of photonic memory, the statistical analysis of the performance of 20 devices for five different memory device types has been summarized in **Table S3**.

Based on the memory performance and photochemistry of the studied photoactive components, we hypothesize, as depicted in **Figure 3**, a plausible working mechanism for the studied memories under light irradiation. As illustrated, both electrets generated Frenkel excitons when illuminated by light; additionally, the left counterpart of the photo-induced electrons was trapped in the electret. After removing the light source, the excited photoactive components underwent dynamic relaxation. **Figure 3** depicts the interlayer exciton generated between the electret and pentacene upon illumination, followed by the trapping of electrons in the PLA electret, resulting in an exceptional memory ratio and current retention. In contrast, the 1.84 eV bandgap between the LUMO level of pentacene and the HOMO level of hemin was too large for their charges to recombine, indicating that the charges trapped in the hemin/PLA electret tend to dissipate through self-charge transfer, resulting in lower memory persistence. In the case of hemin/PLA-based memory, hemin facilitated charge transfer relaxation, and electrons hopped onto adjacent hemin molecules. Some hopping electrons may dissipate during this process.

Therefore, the trapped electrons in the hemin/PLA electret present a challenge in terms of persistence. In addition, the interlayer charge could not recombine due to the significant energy difference between pentacene and hemin. In other words, the interlayer exciton could not form to compensate for the loss of dissipated electrons. Thus, in the case of PPIX/PLA-based memory, PPIX released fluorescence without charge transfer upon relaxation to the ground state, preventing trapped charges' dissipation. Moreover, the proximity of 1.69 eV between the LUMO and HOMO energy levels of pentacene and PPIX provided a driving force to overcome the coulombic force of the bonded charges in pentacene and electret, respectively. Therefore, the interlayer charges recombine and generate additional excitons, suggesting that they were retained in the PPIX/PLA electret after the excitons dissociate. Notably, the intrinsic electron-deficient core of PPIX enabled the consolidation of electron carriers. To further visualize the charged regions of PPIX, its molecular electrostatic potential (ESP) was calculated using density functional theory (**Figure 3**). As observed, the amide group provided a negative ESP region, which suggests that it stabilized negative charges within the electret. Moreover, when the device was driven by photoirradiation, the induced electrons from light illumination and interlayer excitons were preserved well in the PPIX/PLA electret. Consequently, the PPIX/PLA electret derived from the biomass-based PPIX/PLA electret was deemed more favorable for use

in photonic memory. Therefore, the high memory ratio and current retention demonstrate the potential for exceptional discriminability and persistent data storage.

The effect of the distribution of photoactive components on memory performance. By the characteristics mentioned earlier, the natural PPIX, which acts as a photoactive component embedded in a PLA matrix, is advantageous for use as a chargeable electret in a photo memory. Thus, modulating the blending ratio, molecule dispersiveness, specific sizes, and insulating polymer morphology can affect the discreteness of trapping sites, thereby significantly impacting memory performance.[6,33] Therefore, we investigated the memory performance of PPIX/PLA electrets with 1/1, 1/2, and 1/4 blending ratios. All the device performances in this section are summarized in **Table S1**. As demonstrated in **Figure S3**, the electrical stress exerted on all devices resulted in similar switching behaviors. In addition, the transfer curves shifted to the positive region with light exposure of 1 s. Meanwhile, the transient current underwent a significant increase in each device. As anticipated, a more unusual switching behavior was observed with a higher concentration of PPIX in the electret because more electrons were induced by light illumination, and interlayer exciton was retained. In addition, when the exposure interval was set to 1 s, the PPIX composition change modulated

the memory behavior from photo programming to photo recovery. Thus, the increased PPIX composition provided more trapping sites for retaining the induced charges in the electret. Notably, the I_{DS} of the PPIX/PLA(1/1)-based device increased slightly after the light source was removed. This could be attributed to the interlayer excitons generated between PPIX and pentacene upon the removal of light. Consequently, the PPIX/PLA(1/2)-based device had a relatively higher I_{ON}/I_{OFF} than the other two systems, which had I_{ON}/I_{OFF} values of 2.9×10^3 for the PPIX/PLA(1/1)-based device and 1.4×10^3 for the PPIX/PLA(1/4)-based device, respectively. In addition, the adopted blending ratio provided discrete trapping sites, allowing induced charge to be captured or released via an external driving force. To demonstrate this concept, a PPIX/PLA(1/2) electret was prepared for comparison in CF, where PPIX dissolved significantly better than in CF. The surface morphology of the electret was captured by AFM topography, as depicted in **Figure 4a**, and the corresponding transfer and output characteristics are depicted in **Figures 4b** and **S4a**. Thus, it is evident that the PPIX aggregated in the PLA matrix when CF was used as the processing solvent. In addition, the device exhibited a significantly lower I_{ON}/I_{OFF} of 7.3, despite being photo-driven for 60 s, proving the effectiveness of the photoactive component distribution on memory performance.

Based on the mentioned concept, it is, therefore, necessary to specify the purpose of the PLA matrix. In addition to biodegradability and bio-based materials, the ether and carbonyl groups on PLA provide a solid dipole-dipole interaction with the carboxylic acid end group in hemin or PPIX. This strong interaction permits the photoactive components to be firmly encased within the polymer matrix, thereby generating discrete trapping sites in chargeable electrets. To confirm the functionality of PLA, we prepare a control group by blending hydrophobic PPIX with hydrophilic PS.[34-37] **Figure 4c** and **Figure S4b** illustrate the performance of the fabricated device, which exhibits similar V_{TH} shifting but a lower I_{ON}/I_{OFF} of 4.1×10^2 than the PPIX/PLA(1/2)-based device. Due to a larger grain size of grown pentacene (**Figure S5**) on a more hydrophobic surface, the PPIX/PS(1/2)-based device exhibited a greater charge mobility (μ_p) of 5.2×10^{-2} $cm^2V^{-1}s^{-1}$. However, a significant difference in polarity between PPIX and PS resulted in an unfavorable mixing situation, which may reduce the discreteness of trapping sites. As depicted in **Figure 4a**, a PPIX aggregation was observed, and the poorer distribution of photoactive components impacted the photoresponsivity of the electret. The PPIX/PS(1/2)-based device exhibited a lower I_{ON}/I_{OFF} ratio.

The feasibility of bio-electrets and the demonstration of flexible electronics. To further investigate the long-term data storage stability and discriminability, the retention characteristics of the bio-electret-based devices were analyzed (**Figure 5a**). The photo programming procedure was configured as an "ON" state controlled by light illumination for varying exposure times. Hemin/PLA, PPIX/PLA, and PPIX/PS-based devices were illuminated for 60, 5, and 5 s, respectively, to ensure that each electret received adequate charges for stable data recording. In addition, the electrical-erasing processes were set to an "OFF" state, and the devices' memory ratio (I_{ON}/I_{OFF}) was determined from the retained I_{DS} recorded after 10^4 s under a fixed V_D of 60 V and a V_G of 0 V in a dark environment. Devices based on hemin/PLA, PPIX/PLA, and PPIX/PS exhibited I_{ON}/I_{OFF} values of 1.8×10^4, 2.5×10^7, and 2.9×10^6, respectively. Notably, the PPIX/PLA-based device exhibited a higher memory ratio than other devices due to a relatively higher initial I_{ON} recorded at V_G of 0 V and a high retention of I_{ON} after light removal for 10^4 s. The former factor is attributable to the PPIX/PLA electret's high photoresponsivity. As discussed previously, the interlayer exciton formation occurred at the interface of the PPIX/PLA electret and pentacene, producing additional photo-induced charges. In addition, the high degree of PPIX distribution within the PLA matrix validated the discreteness of the trapping sites. These outcomes, therefore, contribute to a higher

photoresponsivity and a greater memory ratio. In addition, the excellent memory resistance could be credited to the unique relaxation dynamic and inherent chemical functionality of PPIX,[27] which enabled the retained charges to consolidate well in its trapping sites. Thus, the I_{ON} remained high, and the PPIX/PLA-based device demonstrated a sustained memory behavior.

To further evaluate the reproducibility of the PPIX/PLA-based devices, writing-reading-erasing-reading switching cycles were performed, as depicted in **Figure S6**, and the averaged I_{DS} of the reading process following photo-writing (ON state) and electrical-erasing (OFF state) in each cycle was recorded in **Figure 5b**. Each cycle was conducted as follows: the device was initially exposed to blue light (405 nm, 0.95 $mWcm^{-2}$), followed by 5 s programming in a constant electrical field (V_G = 0 V and V_D = −60 V). This is referred to as the writing process. Following the removal of the light source, a V_D of −60 V was maintained for the data reading process. A 1 s V_G pulse with a V_D of 60 V was applied for the electrical-erasing process, followed by data reading. The measurements were performed at V_G = 0 V to prevent additional energy consumption during data reading. The PPIX/PLA-based device exhibited stable reversible switching cycles at least 50 times and highly maintained I_{ON} and I_{OFF} averages during the reading process. In addition, the distinct I_{ON}/I_{OFF} was observed to be around three

orders of magnitude. The absence of current decay affirms the decent data discriminability and excellent reliability of the study memories under study.

Based on the advantages mentioned above, PPIX/PLA electret was a promising candidate for integration in next-generation electronic data storage systems. Notably, the PPIX/PLA electret is designed to program in short light intervals to conserve energy, and the biomass derivability and degradability are environmentally friendly to achieve a sustainable economic model.

As depicted in **Figure 5c**, we demonstrate the viability of flexible memories using PPIX/PLA(1/2) as a chargeable electret and PI(ISBA-BPDA) as a bio-polymer substrate and dielectric. Due to the optimized thickness and roughness of the dielectric layer on the PI-based substrate, the photoresponsive performance and the initial mobility of FETs must be considered for the phototransistor memory behavior in flexible devices. Moreover, because hemin and PPIX serve as both photoactive components and hole-trapping sites, the mobility of electrons in this study is lower than the mobility reported in the literature as a whole. Thus, a trade-off between photoresponse and mobility must exist. However, we can optimize the memory performance via well-controlled surface morphology (modulating the blending ratio, processing solvent, and polymer matrix types). In this study, we determined that PPIX/PLA

(2/1) has an excellent memory ratio and current retention characteristics. In addition to describing the initial transfer characteristics and switching behavior under cyclic bending, **Table S2** lists the characteristics. As depicted in **Figure S7a**, the hysteresis phenomenon and output characteristics were recorded. The prepared flexible device exhibits comparable transfer characteristics with an average μ_p of 8.2×10^{-3} $cm^2V^{-1}s^{-1}$, compatible with the conventional silicon-based device described in the previous section. The C_i value of dielectrics fabricated with 302 nm thick PI(ISBA-BPDA) and 285 nm thick PPIX/PLA(1/2) electrets were 8.9 $nFcm^{-2}$. Regarding memory performance, the device exhibited a similar switching behavior during the photo programming process; however, a slight V_{TH} shift was observed during electrical erasure. The low absorbance of the PI(ISBA-BPDA) dielectric at wavelengths longer than 320 nm,[8] precludes the addition of a photoresponsive component to the device. In contrast, the PI(ISBA-BPDA) dielectric may trap some hole carriers from the PPIX/PLA electret, resulting in less conductivity in the active channel and a smaller V_{TH} shift under electrical stress. The flexible device still performed a compatible memory ratio of 1.7×10^3 and 5.0×10^2, before and after 1000 cycles of cyclic bending, respectively, under a bending radius of 5 mm. In addition, an outstanding memory resistance with I_{ON}/I_{OFF} of 8.9×10^5 was observed following a light removal for 10^4 s (**Figure S7b**). The presented results signify the viability of

developing -based flexible memory and offer a promising outlook for bio-derived and biodegradable materials for environmentally friendly optoelectronics.

Conclusions

The current study successfully reports the development of a bio-derived electret-based flexible photonic memory featuring degradability. Examining hemin and PPIX photochemistry, the effect of iron(III) ion insertion on memory performance is investigated for the first time. The hemin/PLA-based electret exhibited an inferior memory performance with a low memory ratio and current retention, despite being photo-driven for a longer duration. In contrast, the PPIX/PLA-based device exhibited a high memory ratio of 8.9×10^5 after light removal for 10^4 s. correspondingly, the mechanism of operation for these two systems was proposed in this study. The presence of the PPIX/PLA electret with the appropriate energy-level alignment to the active layer enabled the generation of interlayer excitons at the interface. In addition, the relaxation dynamic and core structure provided additional sites for charge consolidation. As a result, the device exhibited a higher memory ratio and persistence. In contrast, it was challenging to store charge in hemin because of its self-charge transfer while undergoing relaxation and because the iron(III) ion coordination decreased its trapping sites. On the other

hand, the effect of photoactive component distribution in the polymer matrix was discussed further by varying the blending ratio, processing solvent, and polymer matrix types. As observed, the discreteness of trapping sites considerably influenced the memory ratio. In conclusion, the flexible device based on a PPIX/PLA(1/2) electret demonstrated memory retention even after 1000 cycles of bending with a 5-mm bending radius. This research, therefore, demonstrates the viability of hemin-based bio-electrets in photonic memory and offers the opportunity to replace petroleum-based materials.

Associated Content

Supporting Information.

Supporting Information is available free of charge on the ACS Publications website. Electrochemical characterizations of the photoactive components and polymer; Morphology characterization of the polymer electrets; Field-effect transistor and switching characteristics of the study devices under study.

Author Information

Corresponding Author

*E-mail: T. Satoh (E-mail: satoh@eng.hokudai.ac.jp) and W.-C. Chen (E-mail: chenwc@ntu.edu.tw).

Notes

The authors declare no competing financial interests.

Acknowledgment

The authors appreciate the financial supports by “Hokkaido University President’s Fellowship (Hokkaido University),” “the Photo-excitonic Project (Hokkaido University),” “the Creative Research Institution (Hokkaido University)” and “Advanced Research Center for Green Materials Science and Technology” from the Featured Area Research Center Program within the framework of the Higher Education Sprout Project by the Ministry of Education (109L9006) and the Ministry of Science and Technology in Taiwan (MOST 109-2634-F-002-042).

References

[1] Shi, W.; Guo, Y.; Liu, Y. When Flexible Organic Field-effect Transistors Meet Biomimetics: a Perspective View of The Internet of Things. *Adv. Mater*. **2020**, *32*,1901493.

[2] Amrouch, H.; Chen, J.-J.; Roy, K.; Xie, Y.; Chakraborty, I.; Huangfu, W.; Liang, L.; Tu, F.; Wang, C.; Yayla, M. In Brain-Inspired Computing: Adventure from Beyond CMOS Technologies to Beyond von Neumann Architectures. IEEE/ACM Int. Conf. Comput.-Aided Des. Dig. Tech. Pap. **2021**, 1, 9.

[3] Abbas, S.; Kumar, M.; Ban, D.-K.; Yun, J.-H.; Kim, J. Transparent and Flexible In_2O_3 Thin Film for Multilevel Nonvolatile Photomemory Programmed by Light. *ACS Appl. Electron. Mater*. **2019** 437-443.

[4] Chen, H.; Dong, Z.; Chen, W.; Sun, L.; Du, X.; Zhao, Y.; Chen, P.; Wu, Z.; Liu, W.; Zhang, Y. Flexible and Rewritable Non-Volatile Photomemory Based on Inorganic Lanthanide-Doped Photochromic Thin Films. *Adv. Opt. Mater.* **2020**, *8*,1902125.

[5] Yu, Y.; Ma, Q.; Ling, H.; Li, W.; Ju, R.; Bian, L.; Shi, N.; Qian, Y.; Yi, M.; Xie, L. Small-molecule-based Organic Field-effect Transistor for Nonvolatile Memory and Artificial Synapse. *Adv. Funct. Mater*. **2019**, *29*, 1904602.

[6] Yang, W. C.; Chiang, Y. C.; Lam, J. Y.; Chuang, T. H.; Ercan, E.; Chueh, C. C.; Chen, W. C. Improving the Performance of Nonvolatile Perovskite-Based Photomemory by Size Restrain of Perovskites Nanocrystals in the Hybrid Floating Gate. *Adv. Electron. Mater.* **2020**, *6*, 2000458.

[7] Liao, M.-Y.; Elsayed, M. H.; Chang, C.-L.; Chiang, Y.-C.; Lee, W.-Y.; Chen, W.-C.; Chou, H.-H.; Chueh, C.-C. Realizing Nonvolatile Photomemories with Multilevel Memory Behavior Using Water-processable Polymer Dots based Hybrid Floating Gates. *ACS Appli. Electron. Mater.* **2021**, *3*, 1708-1718.

[8] Chen, C.-K.; Lin, Y.-C.; Ho, J.-C.; Yang, W.-C.; Chen, W.-C. Biomass-Derived Degradable Poly (azomethine) s for Flexible Bistable Photonic Transistor Memories. *ACS Sustainable Chem. Eng.* **2022**, *10*, 5268–5277.

[9] Chang, Y. H.; Ku, C. W.; Zhang, Y. H.; Wang, H. C.; Chen, J. Y. Ultrafast Responsive Non-Volatile Flash Photomemory via Spatially Addressable Perovskite/Block Copolymer Composite Film. *Adv. Funct. Mater.* **2020**, *30*, 2000764.

[10] Lain, H.; Liao, Q.; Yang, Y.; Han, S.T.; Zhou, Y. Optoelectronic Synaptic Transistors Based on Upconversion Nanoparticles. *J. Mater. Chem. C*, **2021,9,640**-648

[11] Mu, B.; Guo, L.; Liao, J.; Zie, P.; Ding, G.; Lv, Z.; Zhou, Y.; Han, S. T.; Yan, Y. Near-infrared Artificial Synapses for Artificial Sensory Neuron System, *Small* **2021**, 17, 2103837.

[12] Jeong, Y. J.; Yun, D.-J.; Noh, S. H.; Park, C. E.; Jang, J. Surface modification of CdSe Quantum Dot Floating Gates for Advancing Light Erasable Organic Field Effect Transistor Memories. *ACS nano* **2018**, *12*, 7701-7709.

[13] Zou, C.; Zheng, J.; Chang, C.; Majumdar, A.; Lin, L. Y. Nonvolatile Rewritable Photomemory Arrays Based on Reversible Phase-change Perovskite for Optical Information Storage. *Adv. Opt. Mater.* **2019**, 7,1900558.

[14] Zhou, L.; Mao, J.; Ren, Y.; Han, S. T.; Roy, V. A.; Zhou, Y. Recent Advances in Flexible Data Storage Devices Based on Organic Nanoscaled Materials. *Small*, 2018, *14*, 1703126.

[15] Taniguchi, M.; Lindsey, J. S. Synthetic Chlorins, Possible Surrogates for Chlorophylls, Prepared by Derivatization of Porphyrins. *Chem. Rev.* **2017** 344–535.

[16] Tsai, M.-C.; Hung, C.-M.; Chen, Z.-Q.; Chiu, Y.-C.; Chen, H.-C.; Lin, C.-Y. The Design of New N-type Porphyrin Acceptors with Subtle Side-chain Engineering for Efficient Nonfullerene Solar Cells with Low Energy Loss and Optoelectronic Response Covering Near-infrared Region. *ACS Appl. Mater. Interfaces* **2019**, *11*, 45991–45998.

[17] Kingsbury, C. J.; Senge, M. O. The Shape of Porphyrins. *Coord. Chem. Rev.* **2021**, *431*, 213760.

[18] Ekrami, M.; Magna, G.; Emam-Djomeh, Z.; Saeed Yarmand, M.; Paolesse, R.; Di Natale, C. Porphyrin-functionalized Zinc Oxide Nanostructures for Sensor Applications. *Sensors* **2018**, *18*, 2279.

[19] Gao, K.; Kan, Y.; Chen, X.; Liu, F.; Kan, B.; Nian, L.; Wan, X.; Chen, Y.; Peng, X.; Russell, T. P. Low-bandgap Porphyrins for Highly Efficient Organic Solar Cells: Materials, Morphology, and Applications. *Adv. Mater.* **2020**, *32*, 1906129.

[20] Ou, Q.; Yang, B.; Zhang, J.; Liu, D.; Chen, T.; Wang, X.; Hao, D.; Lu, Y.; Huang, J. Degradable Photonic Synaptic Transistors Based on Natural Biomaterials and Carbon Nanotubes. *Small* **2021**, *17*, 2007241.

[21] Zhang, J.;Liu, D.;Ou, Q.;Lu, Y.;Hang, J. Covalent Coupling of Porphyrins with Monolayer Graphene for Low-Voltage Synaptic Transistors. *ACS Appl. Mater. Interfaces* **2022**, *14*, 11699–11707.

[22] Wang, X.; Lu, Y.; Zhang, J.; Zhang, S.; Chen, T.; Ou, Q.; Huang, J. Highly Sensitive Artificial Visual Array Using Transistors Based on Porphyrins and Semiconductors. *Small* **2021**, *17*, 2005491.

[23] Sjodt, M.;Macdonald, R.;Marshall, J. D.;Clayton, J.;Olson, J. S.;Phillips, M.;Gell, D. A.;Wereszczynski, J.;Clubb, R. T. Energetics Underlying Hemin Extraction from Human Hemoglobin by Staphylococcus Aureus. *J. Biol. Chem.* **2018** 6942–6957.

[24] Mahawar, L.; Popek, R.; Shekhawat, G. S.; Alyemeni, M. N.; Ahmad, P. Exogenous Hemin Improves Cd2+ Tolerance and Remediation Potential in Vigna Radiata by Intensifying the HO-1-mediated Antioxidant Defense System. *Sci. Rep.* **2021,11,12**.

[25] Zhou, Y.-C.; Ran, X.-X.; Chen, A.-Y.; Chai, Y.-Q.; the Yuan, R.; Zhuo, Y. Efficient Electrochemical Self-catalytic Platform Based on L-Cys-hemin/G-quadruplex and Its Application in Bioassays. *Anal. Chem.* **2018** 9109–9116.

[26] Alsharabasy, A. M.; Pandit, A.; Farràs, P. Recent Advances in the Design and Sensing Applications of Hemin/Coordination Polymer-Based Nanocomposites. *Adv. Mater*. **2021**, *33*, 2003883.

[27] Marcelli, A.; Foggi, P.; Moroni, L.; Gellini, C.; Salvi, P. R. Excited-state Absorption and Ultrafast Relaxation Dynamics of Porphyrin, Diprotonated Porphyrin, and Tetraoxaporphyrin Dication. *J. Phys. Chem.* **2008** 1864–1872.

[28] Sun, C.;Hu, B.;Zhou, W.;Xu, S.;Liu, Z. Investigations on the Demetalation of Metalloporphyrins under Ultrasound Irradiation. *Ultrason. Sonochem.* **2011**, *18*, 501-505.

[29] Marcelli, A.;Badovic, I. J.;Orlic, N.;Salvi, P. R.; Gellini, C. Excited-state Absorption and Ultrafast Relaxation Dynamics of Protoporphyrin IX and Hemin. *Photochem. Photobiol. Sci.* **2013**, *12*, 348-355.

[30] Carmeli, I.;Liverman, I.;Kramersky, L.;Fan, Z.;Gogorov, A. O.;Markovich, G.;River, S. The Broad Band Enhancement of Light Absorption in Photosystem I by Metal Nanoparticle Antennas. *Nano Lett.* **2010**, *10*, 2069-2074.

[31] Jiang, D. H.; Satoh, T.; Tung, S. H.; Kuo, C.-C. Sustainable Alternatives to Nondegradable Medical Plastics. *ACS Sustainable Chem. Eng.* **2022**, *10*, 4792–4806.

[32] Chen, C.K.; Lin, Y.C.; Hsu, L.C.; Ho, J.C.; Ueda, M.; Chen, W.-C. High Performance Biomass Based Polyimides for Flexible Electronic Applications. *ACS Sustainable Chem. Eng.* **2021**, *9*, 3278-3288.

[33] Lin, Y.C.; Yang, W.C.; Chiang, Y.C.; Chen, W.-C. Recent Advances in Organic Phototransistors: Nonvolatile Memory, Artificial Synapses, and Photodetectors. *Small Sci.* **2022**, *2*, 2100109.

[34] Ke, C. Y.; Chen, M. N.; Chen, M. H.; Li, Y. T.; Chiu, Y. C.; Liou, G. S. Novel Authentic and Ultrafast Organic Photorecorders Enhanced by AIE-Active Polymer Electrets via Interlayer Charge Recombination. *Adv. Funct. Mater.* **2021**, *31*, 2101288.

[35] Chen, Y.-C.; Lin, Y.-C.; Hsieh, H.-C.; Hsu, L.-C.; Yang, W.-C.; Isono, T.; Satoh, T.; Chen, W.-C. Improving the Performance of Photonic Transistor Memory Devices Using Conjugated Block Copolymers as Floating Gate. *J. Mater. Chem. C* **2021**, *9*, 1259-1268.

[36] Zhang, Q.; Kale, T. S.; Plunkett, E.; Shi, W.; Kirby, B.; Reich, D. H.; Katz, H. E. Highly Contrasting Static Charging and Bias Stress Effects in Pentacene Transistors with Polystyrene Heterostructures Incorporating Oxidizable N, N′-Bis (4-methoxyphenyl) aniline Side Chains as Gate Dielectrics. *Macromolecules* **2018** 6011–6020.

[37] Ren, Z.;Guo, R.;Bi, H.;Jia, X.;Xu, M.;Cai, L. Interfacial Adhesion of Polylactic Acid on Cellulose Surface: a Molecular Dynamics Study. *ACS Appl. Mater. Interfaces* **2019**, *12*, 3236–3244.

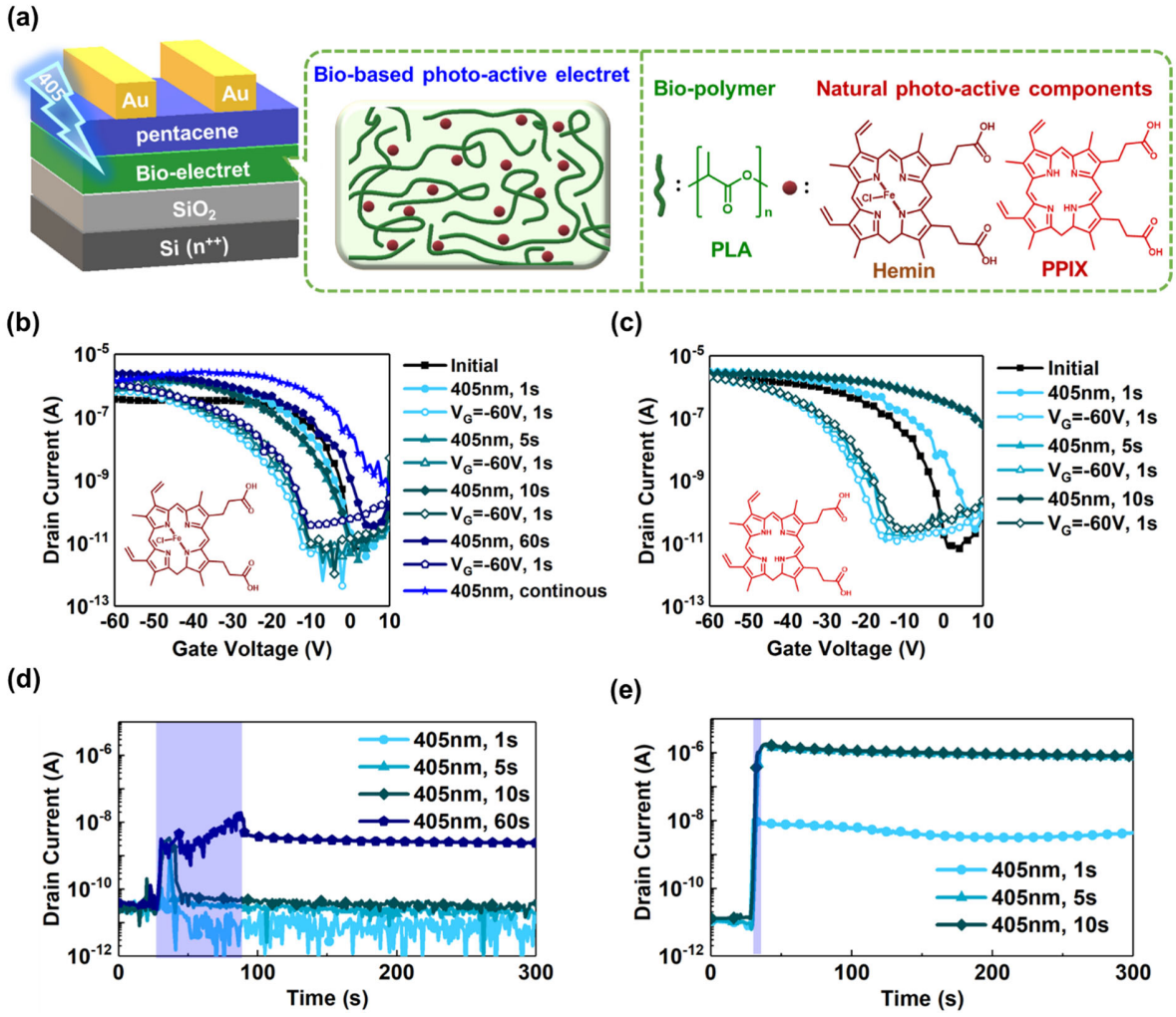

Figure 1. (a) Schematic illustration of the photo memory of the bio-based photoactive electrets. I–V curves of the photonic FET memory based on (b) hemin/PLA and (c) PPIX/PLA electret with V_D = -60 V under photo-writing (405 nm, 0.95 mWcm^{-2}, various time interval) and electrical-erasing (V_g = -60 V, 1 s). Transient characteristics based on (d) hemin/PLA and (e) PPIX/PLA electrets performed in a dark environment instead of light illumination process.

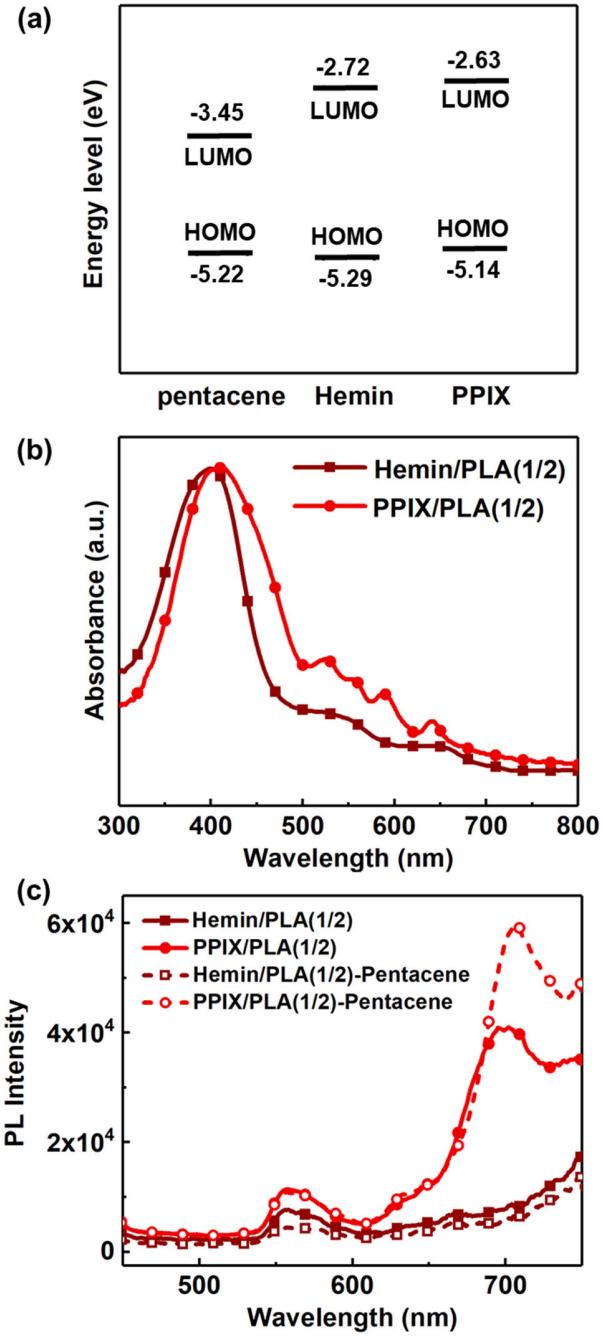

Figure 2. (a) Band diagram of pentacene, hemin, and PPIX. (b) Ultraviolet−visible spectra of the study bio-electrets under study. (c) Photoluminescence spectra of bio-electret (solid line) and pentacene/bio-electret bilayer (dash line) under an excitation wavelength of 450–750 nm.

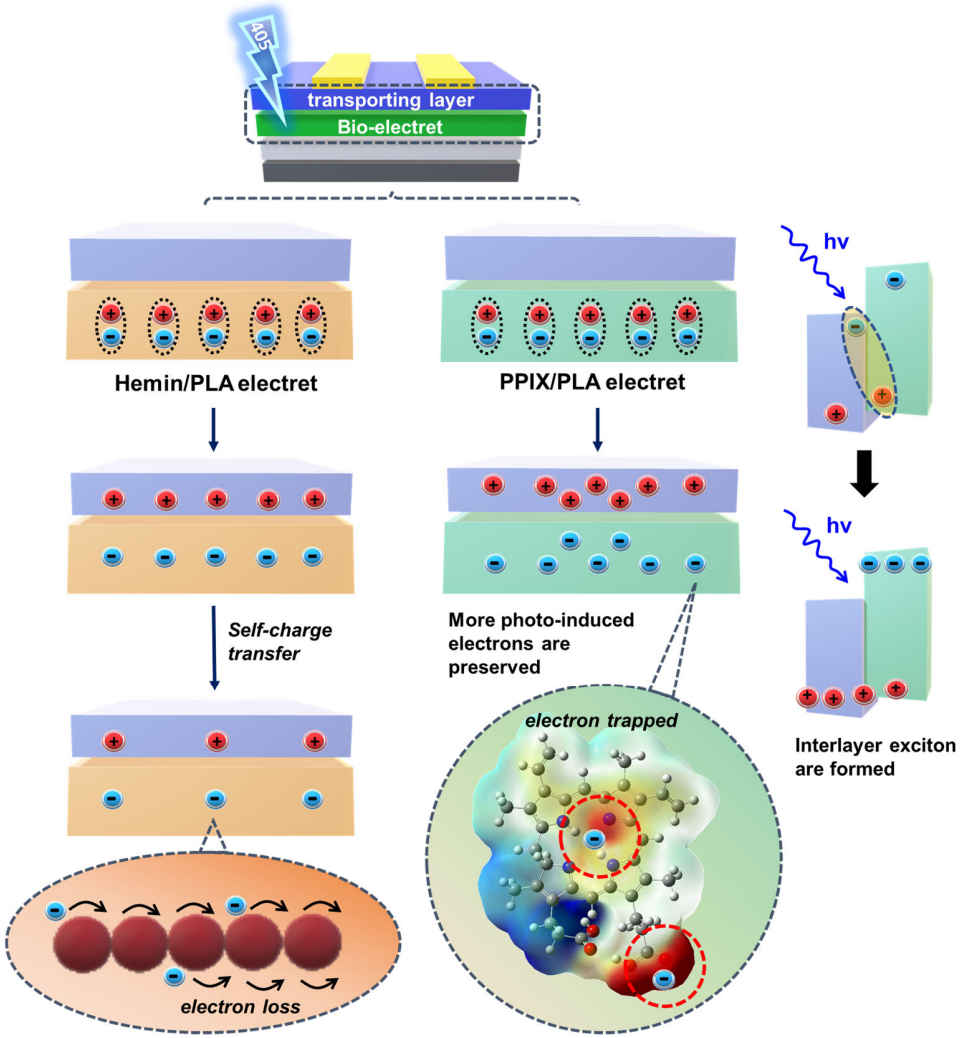

Figure 3. Schematic illustrations depicting the working mechanism of hemin/PLA and PPIX/PLA-based memories under light illumination and removal of light source. Optimization of PPIX by density functional theory and ESP on the 0.02 a.u. contours of the electronic density of three repeating units. The negative ESP regions are denoted in red and the positive regions are denoted in blue.

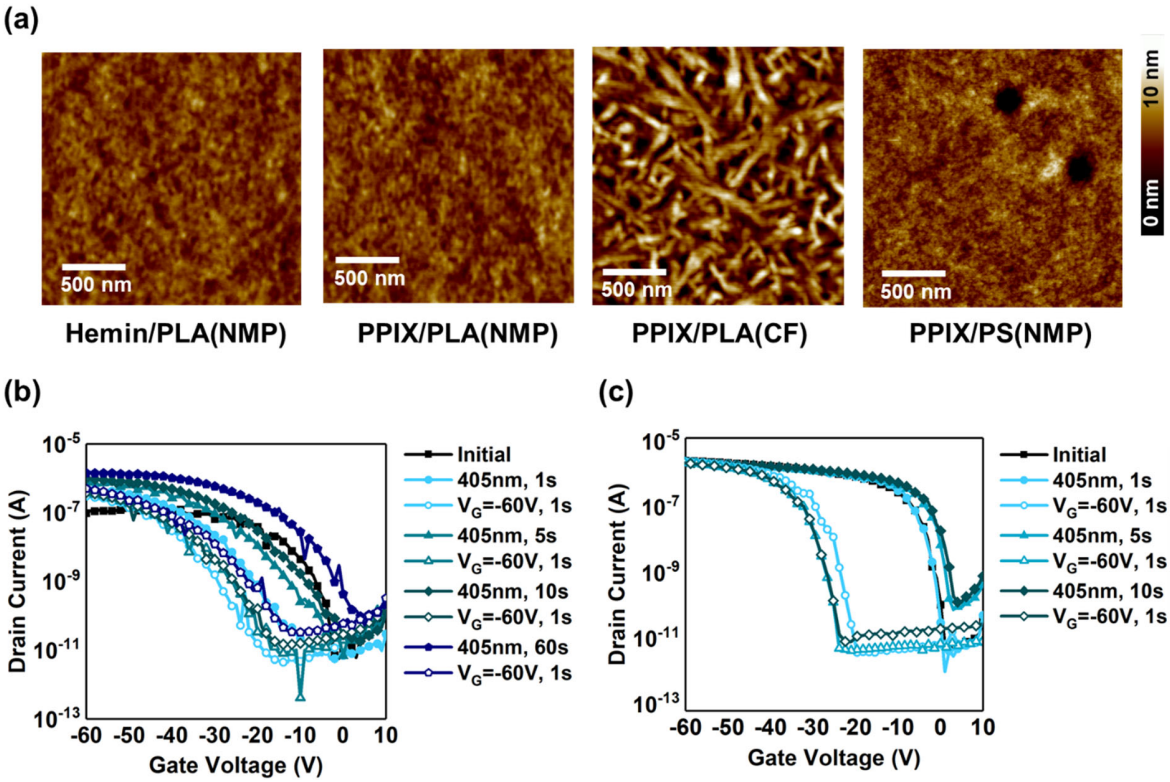

Figure 4. (a) Atomic force microscopy height images (2 × 2 μm) of the chargeable electret fabricated using photoactive components/polymer matrix at a blending ratio of 1/2. The processing solvent is denoted in brackets. I–V curves of the photonic field-effect transistor memory based on (b) PPIX/PLA(CF) and (c) PPIX/PS(NMP) electret with V_D = -60 V under photo-writing (405 nm, 0.95 mWcm^{-2}, various of time interval) and electrical erasing (V_g = −60 V, 1 s).

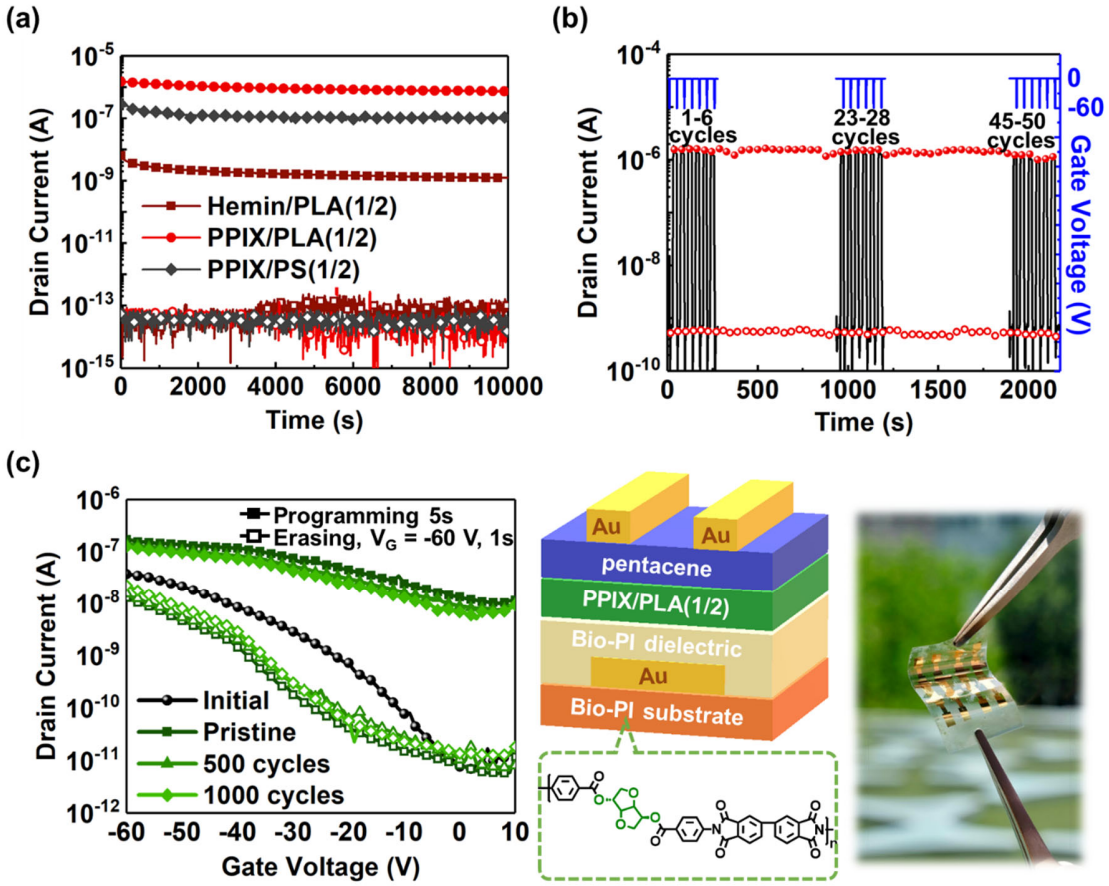

Figure 5. (a) Retention characteristics of memories studied in the ON state (photo-writing under light illumination at 405 nm for various intervals) and the OFF state (electrical-erasing under V_G of -60 V pulse for 1 s). Hemin/PLA, PPIX/PLA, and PPIX/PS-based devices were illuminated for 60, 5, and 5 s, respectively. (b) Endurance characteristics of the PPIX/PLA(1/2)-based device with continuous writing-reading-erasing-reading cycles. The averaged I_{DS} of the reading process after photo-writing (ON state) and electrical erasing (OFF state) in each cycle are depicted. (c) Memory switching behaviors of a flexible device

fabricated using PI(ISBA-BPDA) as the substrate and dielectric, PPIX/PLA(1/2) as the electret, and pentacene as the active layer.

For Table of Contents use only